Journal of the Meteorological Society of Japan, Vol. 85A, pp. 229–242, 2007

Auto-calibration System Developed to Assimilate AMSR-E Data into a Land Surface Model for Estimating Soil Moisture and the Surface Energy Budget

Kun YANG, Takahiro WATANABE, Toshio KOIKE

Department of Civil Engineering, The University of Tokyo, Tokyo, Japan

Xin LI

Cold and Arid Regions Environmental and Engineering Research Institute, CAS, Lanzhou, China

Hideyuki FUJII, Katsunori TAMAGAWA

Department of Civil Engineering, The University of Tokyo, Tokyo, Japan

Yaoming MA

Institute of Tibetan Plateau Research, CAS, Beijing, China

and

Hirohiko ISHIKAWA

Disaster Prevention Research Institute, Kyoto University, Kyoto, Japan

(Manuscript received 23 February 2006, in final form 31 August 2006)

Abstract

Low-frequency microwave brightness temperature is strongly affected by near-surface soil moisture; therefore, it can be assimilated into a land surface model to improve modeling of soil moisture and the surface energy budget. This study presents a new variational land system used to assimilate AMSR-E brightness temperature of vertical polarization of 6.9 GHz and 18.7 GHz. The system consists of a land surface model (LSM) used to calculate surface fluxes and soil moisture, a radiative transfer model (RTM) to estimate the microwave brightness temperature, and an optimization scheme to search for optimal values of soil moisture by minimizing the difference between modeled and observed brightness temperature. The LSM is an improved simple biosphere model for sparse vegetation modeling and the RTM is a Q-h model that can account for the effects of surface roughness and vegetation. Several parameters in the LSM and RTM can significantly affect the outputs of the land data assimilation system but their values are either highly variable or unavailable. To solve this problem, we developed a dual-pass assim-

Corresponding author: Toshio Koike, Dr., Professor, River Lab, Department of Civil Engineering, The University of Tokyo, Hongo 7-3-1, Bunkyo-ku, Tokyo 113-8656, Japan.
E-mail: tkoike@hydra.t.u-tokyo.ac.jp; yangk@hydra.t.u-tokyo.ac.jp
© 2007, Meteorological Society of Japan

ilation technique. Pass 1 inversely estimates the optimal values of the model parameters with long-term (~months) forcing data and brightness temperature data, while Pass 2 estimates the near-surface soil moisture in a daily assimilation cycle. This system is driven by well-established reanalysis data and global data sets of leaf area index, precipitation, and surface radiation, and was tested at a CEOP (Coordinate Enhanced Observing Period) reference site on the Tibetan Plateau. The system not only detected the effect of precipitation events that were missing in the forcing data, but also led to a significant improvement in modeling of the surface energy budget.

1. Introduction

Land–atmosphere interactions are realized via exchanges of water, energy, and carbon at the land surface. Estimating the surface energy budget is a topic of great importance for studies of hydrological and atmospheric processes. The energy budget can be observed at a patch scale or estimated for a regional scale by combining satellite infrared data with surface meteorological data for clear skies (Ma et al. 2002; Ma et al. 2003), but it is difficult to produce continuous temporal and spatial variations without referring to soil moisture.

As a controller of surface energy partitioning between sensible heat and latent heat, soil moisture plays an important role in land–atmosphere interactions (Entekhabi et al. 1996; Betts et al. 1996; Betts 2004). This is especially true in semi-arid regions where soil moisture memory may affect precipitation at a seasonal scale (Koster et al. 2004); however, the high degree of spatial variability in soil moisture makes it extremely difficult to observe its spatial distribution. Soil moisture simulated by state-of-the-art land surface models is model-dependent even when driven by identical forcing data, as demonstrated by the Global Soil Wetness Project (Dirmeyer et al. 1999), the Project for Inter-comparison of Land-Surface Parameterization Schemes (Pitman et al. 1999), and the Coordinated Enhanced Observing Period (CEOP) model inter-comparison study (Yang et al., this issue).

Soil moisture can also be remotely sensed from satellite infrared data (Wetzel et al. 1984; Gillies and Carlson 1995) in areas where surface temperature is controlled by thermal inertial. Soil moisture is also retrievable from low-frequency microwave data (Jackson 1993; Wigneron et al. 1995; Njoku and Entekhabi 1996; Burke and Simmonds 2001; Owe et al. 2001; Paloscia 2001), as high-frequency (>19 GHz) passive microwave polarization differences are sensitive to vegetation but not soil moisture (Prigent et al. 2005; Vinnikov et al. 1999).

Land data assimilation (the merging of information from satellites, ground-based stations, and models) is perhaps the only effective way to obtain estimates of soil moisture and surface energy fluxes with the accuracy and coverage required for hydrologic and meteorological applications (Margulis et al. 2002). Previous studies have demonstrated that satellite-retrieved soil moisture can add skill to the forecasting of the land-surface response to precipitation (Pauwels et al. 2001; Crow et al. 2005). Reichle and Koster (2005) also demonstrated that the assimilation product is superior to both satellite data and model data when these data sets are considered in isolation. A land data assimilation system can assimilate a variety of data into land surface models, including surface skin temperature (van den Hurk 2001; Meng et al. 2003), near-surface soil moisture (Parada and Liang 2004; Zhang et al. 2006), and microwave brightness temperature (Houser et al. 1998; Crosson et al. 2002). Recently, mathematical methods such as variational and sequential data assimilation have been widely addressed and applied (e.g., Reichle et al. 2001; Pathmathevan et al. 2003; Dunne and Entekhabi 2005).

Soil moisture and the surface energy budget are sensitive to model parameters for both land-surface models (Yang et al. 2005) and data assimilation systems (Robock et al. 2003). Although this sensitivity to parameters has been widely addressed for land surface modeling, few studies have considered this issue in terms of land-data assimilation. The North American Land Data Assimilation System (NLDAS; Mitchell et al. 2004) and the Global Land Data Assimilation System (GLDAS; Rodell et al. 2004) use available data sets of soil

parameters, and the applicability of these data sets requires justification.

In this study, we present a variational land-data assimilation system developed at the University of Tokyo (LDAS-UT). The system assimilates AMSR-E low-frequency data into a land surface model to estimate the soil moisture and the surface energy budget. LDAS-UT embeds a dual-pass technique: the first pass estimates model parameters using long-term (~months) satellite data and forcing data, and the second pass estimates soil moisture and the surface energy budget by assimilating daily satellite data.

The remainder of this paper is organized as follows. Section 2 provides a description of LDAS-UT, and Section 3 introduces the driving data. A case study undertaken at a CEOP (Koike 2004) reference site is described in Section 4, and a summary of the study is presented in Section 5.

2. LDAS-UT

LDAS-UT consists of a land surface model (LSM) used to calculate fluxes and soil moisture, a radiative transfer model (RTM) to estimate microwave brightness temperatures (T_b) from surface temperature and soil moisture, and an optimization scheme to search for optimal values of parameters and near-surface soil moisture by minimizing the difference between modeled and observed brightness temperatures.

2.1 Algorithm

Figure 1 shows the LDAS-UT algorithm, which includes a dual-pass assimilation technique. Both passes assimilate observed brightness temperatures of the vertical polarization at a lower frequency (6.9 GHz) and a higher frequency (18.7 GHz). This choice is critical in terms of producing stable and reliable estimates of soil moisture. The vertical polarization is more desirable than the horizontal polarization because it is relatively insensitive to vegetation coverage (this conclusion can be drawn from the measurements and modeling results of Fujii 2005). As the lower frequency T_b is much more sensitive to near-surface soil moisture than the higher frequency, their difference is correlated with soil wetness (Koike et al. 2000). A soil wetness index (SWI) is then defined by $SWI = 2(T_b^{18.7V} - T_b^{6.9V})/(T_b^{18.7V} + T_b^{6.9V})$. A high SWI value corresponds to a wet surface, and a low value to a dry surface.

Estimating brightness temperatures using RTM requires the input of near-surface soil water content (w_1), ground temperature (T_g), canopy temperature (T_c), vegetation water content (VWC), canopy parameters, surface roughness parameters, and soil texture (see Section 2.3). The simulation of surface variables (w_1, T_g, T_c) using a LSM also requires a number of soil and vegetation parameters (see Section 2.4). The modeled T_b is thus sensitive to several parameters used in the LSM and RTM. In Pass 1, these parameters are obtained by minimizing a cost function that accounts for the difference between modeled and observed long-term brightness temperatures (t_{pass1}; scale of ~months). The cost function includes an observation error term and a background error term. The observation error term is defined by

$$F_{obs} = \sum_{t=0}^{t_{pass1}} [(T_{b,est}^{6.9V} - T_{b,obs}^{6.9V})^2 + (T_{b,est}^{18.7V} - T_{b,obs}^{18.7V})^2], \quad (1)$$

where the subscript obs denotes the observed value and est is the modeled value.

In Pass 1, the background error term is not directly accounted for in the cost function; instead, it is realized via an adjustment of near-surface soil water content (w_1) at each observing time such that the recalculated SWI value, which depends on w_1, is close to $(SWI_{est} + SWI_{obs})/2$. Note that this adjustment is implemented after (rather than before) adding the bias term $(T_{b,est} - T_{b,obs})^2$ into Eq. (1) (see details in Fig. 1). The existence of model deficiencies and errors in the forcing data mean that simulated soil moisture may become unrealistic without this adjustment, resulting in the absence of a correlation between $T_{b,est}$ and $T_{b,obs}$ regardless of how the parameter values are tuned. Accordingly, this adjustment is critical in terms of optimizing the parameters.

The optimal parameter values are then transferred into Pass 2 for retrieving soil moisture and the surface energy budget by assimilating the brightness temperature into the LSM. Pass 2 only optimizes the near-surface

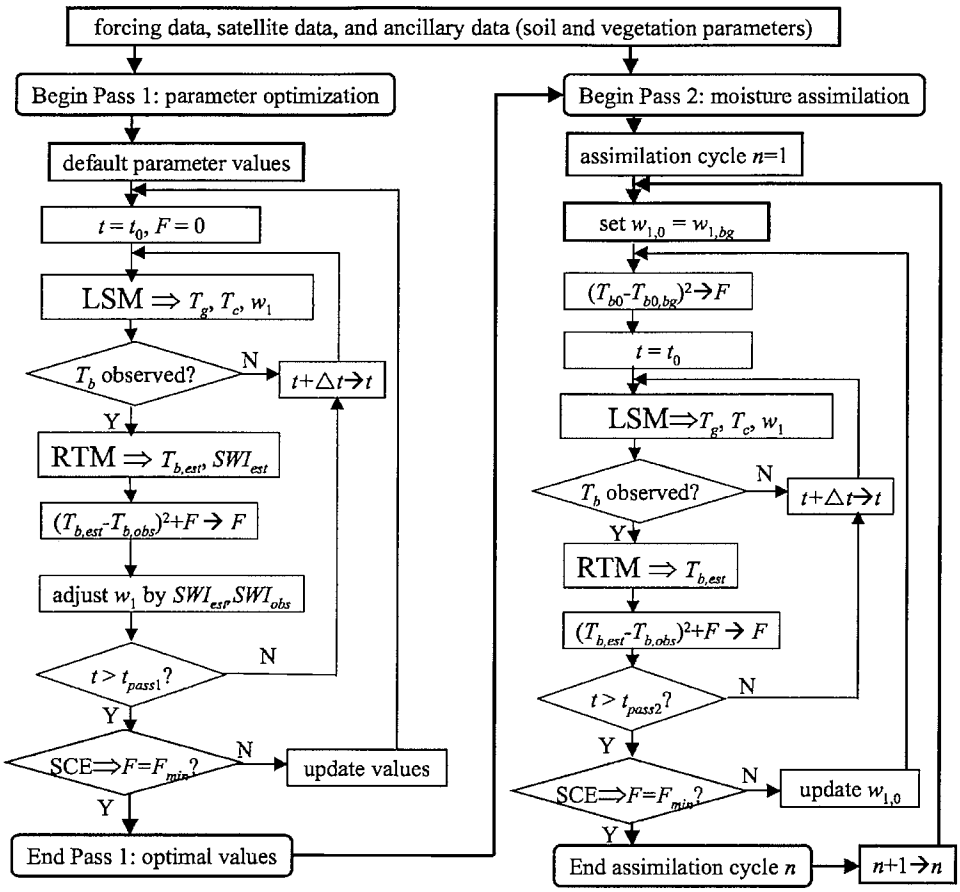

Fig. 1. Algorithm used in LDAS-UT. t is the time; T_g, T_c, and w_1 are the ground temperature, canopy temperature, and near-surface soil water content, respectively; T_b is the brightness temperature; and SWI is the soil wetness index. The subscript *0* denotes the initial value, *obs* denotes the observed value, *est* is the estimated value, and *bg* is the background value. SCE is a global minimization scheme (Duan et al. 1993).

soil moisture, and its assimilation window (t_{pass2}; ~1 day) is much shorter than that for Pass 1. The cost function for Pass 2 is defined by

$$F_{obs} = \sum_{t=0}^{t_{pass2}} [(T_{b,est}^{6.9V} - T_{b,obs}^{6.9V})^2 + (T_{b,est}^{18.7V} - T_{b,obs}^{18.7V})^2] + [(T_{b0,bg}^{6.9V} - T_{b0}^{6.9V})^2 + (T_{b0,bg}^{18.7V} - T_{b0}^{18.7V})^2], \quad (3)$$

where $T_{b0,bg}$ and T_{b0} are the simulated brightness temperature at the initial time of each assimilation cycle using the background value of $w_{1,0}$ (i.e., $w_{1,bg}$) and the renewed $w_{1,0}$ value, respectively.

Pass 1 requires just a single execution because the optimized parameters only include static model parameters and initial soil water conditions. It can be implemented using previous data prior to the real-time assimilation of satellite data in Pass 2.

2.2 *Land surface model*

The land surface model is a simple biosphere model (SiB2) developed by Sellers et al. (1996a). This model includes one canopy layer and three soil layers and describes canopy radiative transfer, aerodynamic canopy transfer, and conductance-photosynthetic processes. The model is a typical dual-source model that pa-

rameterizes heat transfer from both the canopy and the ground. Although SiB2 succeeds in describing dense-canopy processes, it requires further improvements to successfully model sparse-canopy processes.

For a sparse canopy, the heat transfer from the ground can be a dominant term in the total heat fluxes. Therefore, it is important to appropriately parameterize the ground heat fluxes. A number of studies have recorded significant differences between momentum transfer resistance and heat transfer resistance; it is therefore necessary to discriminate the aerodynamic roughness length z_0 and the thermal roughness length z_T. In this study, the following scheme was introduced to SiB2 for modeling ground heat fluxes:

$$z_T = \frac{70\nu}{u_*} \exp(-\beta u_*^{1/2} |T_*|^{1/4}), \tag{3}$$

where $\beta = 7.2\ \mathrm{m}^{-1/2}\ \mathrm{s}^{1/2}\ \mathrm{K}^{-1/4}$, u_* [m s^{-1}] is the friction velocity, T_* [K] is a temperature scale defined as $-H/\rho c_p u_*$, and ν [m^2 s^{-1}] is the air kinematic viscosity. H [W m^{-2}] is the sensible heat flux, ρ [kg m^{-3}] is the air density, $c_p = 1004$ J kg^{-1} K^{-1}, $\nu = \nu_0 \left(\frac{p_0}{p}\right)\left(\frac{T}{T_0}\right)^{1.754}$, $\nu_0 = 1.328 \times 10^{-5}$ m^2 s^{-1}, $p_0 = 1.013 \times 10^5$ Pa, and $T_0 = 273.15$ K.

Equation (3) is a revised version of the scheme proposed by Yang et al. (2002). The original scheme uses potential temperature to calculate heat fluxes, but SiB2 uses temperature. Accordingly, we adjusted β in Eq. (3) from 10 to 7.2. We recently evaluated this scheme and several other commonly quoted formulas using flux data derived from eight field experiments in arid and semi-arid regions; the fluxes parameterized using Eq. (3) were generally in good agreement with observations.

A further improvement is the canopy model used for heat and momentum transfer. Theoretically, the value of the aerodynamic roughness length for a very sparse canopy (i.e., leaf area index or vegetation coverage $\to 0$) should approach the roughness length of the ground beneath the canopy; however, the SiB2 model produces a much smaller length than that of the ground beneath the canopy because the model is incompatible with traditional mixing-length theory. For an improved description of sparse-canopy processes, we replaced the SiB2 canopy model with a new model (Watanabe and Kondo 1990) that is compatible with mixing-length theory.

2.3 *Radiative transfer model*

Microwave brightness temperature is given by

$$\begin{aligned} T_{bp} = {} & T_g(1-\Gamma_p)\exp(-\tau_c) \\ & + T_c(1-\omega)[1-\exp(-\tau_c)] \\ & \times [1+\Gamma_p \exp(-\tau_c)], \end{aligned} \tag{4}$$

where the subscript p denotes polarization (vertical or horizontal), Γ_p is soil reflectivity, τ_c is the optical thickness of the vegetation, and ω is the single-scattering albedo of the vegetation.

The soil reflectivity can be calculated using a Q-h model (Wang and Choudhury 1981) or a Q-p model (Shi et al. 2005); we chose to use a Q-h model:

$$\Gamma_p = [(1-Q)\cdot R_p + Q \cdot R_q]\exp(-h), \tag{5}$$

where the subscripts p and q denote vertical and horizontal polarization, respectively, Q and h are empirically determined surface roughness parameters, and R is the Fresnel power reflectivity that describes the soil reflectivity of a smooth surface.

The horizontal (R_h) and vertical (R_v) Fresnel power reflectivity are calculated by

$$R_h = \left|\frac{\cos\theta - \sqrt{\varepsilon_r - \sin^2\theta}}{\cos\theta + \sqrt{\varepsilon_r - \sin^2\theta}}\right|^2, \tag{6a}$$

$$R_v = \left|\frac{\varepsilon_r\cos\theta - \sqrt{\varepsilon_r - \sin^2\theta}}{\varepsilon_r\cos\theta + \sqrt{\varepsilon_r - \sin^2\theta}}\right|^2, \tag{6b}$$

where θ is the incident angle and ε_r is the soil dielectric constant.

The soil dielectric constant follows Dobson et al. (1985):

$$\varepsilon_r = [1 + (1-w_s)(\varepsilon_s^\alpha - 1) + w^\beta \varepsilon_{fw}^\alpha - w]^{1/\alpha}, \tag{7}$$

where w_s is the soil porosity, w is the soil water content, $\varepsilon_s = (4.7, 0.0)$ is the dielectric constant of a very dry soil, ε_{fw} is the dielectric constant of free water, $\alpha = 0.65$, and β is a soil-texture-dependent coefficient.

The coefficient β is determined from the soil texture (Ulaby et al. 1986):

$$\begin{aligned} \beta = {} & 1.09 - 0.0011 \times \%sand \\ & + 0.0018 \times \%clay, \end{aligned} \tag{8}$$

where *%sand* and *%clay* are the percentage of sand and clay in the soil, respectively.

The model parameters in Eqs. (4) and (5) are frequency-dependent and are given by

$$h = (k \cdot s)^{\sqrt{0.1 \cos\theta}}, \tag{9}$$

$$Q = Q_0 (k \cdot s)^{0.975}, \tag{10}$$

$$\tau_c = b'(100\lambda)^{\chi} w_c / \cos\theta, \tag{11}$$

$$\omega = 0.00083/\lambda, \tag{12}$$

where λ [m] is the wavelength, k is the wave number defined as $2\pi/\lambda$, s is the standard deviation of surface height, w_c [kg m^{-2}] is the vegetation water content, and Q_0, b', and χ are empirical coefficients.

Equation (9) follows Wegmuller and Matzler (1999), while Eq. (11) follows Jackson and Schmugge (1991). Equations (10) and (12) were fitted from the limited measurements provided by Fujii (2005). The value of χ depends on vegetation type (leaf dominated, stem-dominated, or grasses), and Jackson and Schmugge (1991) suggested values of -1.08 for wheat (stem-dominated) and -1.38 for soybean (leaf-dominated).

The vegetation water content is estimated by (Paloscia and Pampaloni 1988)

$$w_c = \exp(LAI/3.3) - 1, \tag{13}$$

where LAI [m^2 m^{-2}] is the leaf area index.

2.4 *Model parameters*

The system imports several global data sets to provide the parameters required in the LSM and the RTM. The default values of soil parameters (thermal and hydraulic properties) are derived from $1° \times 1°$ ISLSCP (International Satellite Land Surface Climatology Project) Initiative II soil data (Global Soil Data Task 2000), and values of vegetation parameters (classification and coverage) are derived from $1° \times 1°$ ISLSCP Initiative II vegetation data (Loveland et al. 2001). Other vegetation parameters are taken directly from Sellers et al. (1996b).

The high spatial variability of soil properties means that ISLSCP soil data can only provide a background value for soil texture and soil parameters. In addition, RTM parameters (surface roughness parameters and vegetation optical parameters) and values of initial soil moisture are usually unavailable. These values are determined in Pass 1. Considering the instability of the solutions and computational cost, it is important to reduce the number of optimized parameters by considering the following empirical relationships between soil texture and soil parameters:

$$\rho_s c_s = [0.076 + 0.748\rho_d/\rho_w] \times 10^6 + 4.195 \times 10^6 w \tag{14}$$

$$\lambda_s = \lambda_d + (\lambda_m - \lambda_d)\exp[0.36(1 - 1/w)] \tag{15a}$$

$$\lambda_m = 0.5^{w_s} \times (7.7^{0.01\times\%sand} 2.0^{1-0.01\times\%sand})^{1-w_s} \tag{15b}$$

$$\lambda_d = (0.135\rho_d + 64.7)/(2700 - 0.947\rho_d) \tag{15c}$$

$$K_s = 7.0556 \times 10^{-6.884+0.0153\times\%sand} \tag{16}$$

$$\psi_s = -0.01 \times 10^{1.88-0.0131\times\%sand} \tag{17}$$

$$b = 2.91 + 0.159 \times \%clay \tag{18}$$

where w is the soil water content; $\rho_s c_s$ [J K^{-1} m^{-3}] is the soil heat capacity; λ_s [W m^{-1} K^{-1}] is the thermal conductivity of the soil; K_s [m s^{-1}], ψ_s [m], and b are the hydraulic parameters of Clapp and Hornberger (1978); ρ_d [kg m^{-3}] is the bulk density of a dry soil calculated using $\rho_d = \rho_s(1 - w_s)$ and $\rho_s = 2650$ kg m^{-3}; and $\rho_w = 1000$ kg m^{-3}.

Equations (14), (15), and (16–18) follow the Global Soil Data Task (2000), the formula proposed by Johansen (1975) and revised by Yang et al. (2005), and Cosby et al. (1984), respectively. As all of the soil thermal and hydraulic parameters can be estimated from soil texture using Eqs. (14–18), the parameters to be optimized include soil porosity (w_s), soil texture (*%sand*, *%clay*), surface roughness parameters (s and Q_0), the vegetation parameter (b'), and the initial water content of the three soil layers (w_1, w_2, w_3). These values are optimized by minimizing the cost function (Eq. 1) using the effective and efficient Shuffled Complex Evolution method developed by Duan et al. (1993). The upper and lower bounds required for this optimization are sourced from Global Soil Data Task (2000).

3. LDAS-UT driving data

The LDAS-UT grid size is set to $0.5° \times 0.5°$, which is comparable to the footprint of the lowest-frequency AMSR-E data. Driving a land data assimilation requires a comprehensive set of atmospheric forcing data at consistent tem-

poral and spatial scales. A major effort of GLDAS and NLDAS is to improve the forcing data, whose quality crucially affects LDAS output (Luo et al. 2003; Berg et al. 2003). LDAS-UT is driven by three data sets: 1° × 1° GPCP (Global Precipitation Climatology Project) precipitation data (Huffman et al. 2001), 2.5° × 2.5° ISCCP downward radiation data (Zhang et al. 2004), and 1.5° × 1.5° NCEP (National Centers for Environmental Prediction) reanalysis data (wind, temperature, and humidity). The existence of biases in certain regions means that the NCEP data require correction using in situ data before being interpolated to LDAS-UT grids. Leaf area index data is sourced from MODIS 0.25° × 0.25° gridded 8-day leaf area index products (Knyazikhin et al. 1999).

4. Case study at a CEOP reference site

The BJ CEOP reference site in East Tibet was established by the CEOP Asia–Australia Monsoon Project in Tibet (CAMP-Tibet) in 2003. The site is located within the assimilation grid centered at 91.75°E, 31.25°N. For convenience of description, the grid is herein termed a CEOP grid. The site is relatively flat and covered with sparsely distributed short grass during the rainy season (June–August). The CAMP-Tibet Project collected a large amount of data in this 0.5° × 0.5° grid in 2003. The stations are shown in Fig. 2, and items measured for the case study are listed in Table 1. To evaluate the capability of LDAS-UT, we compared the results of two case studies with in situ data for the period from May (pre-monsoon) to September (post-monsoon). One of the case studies is a dual-pass assimilation case and the other is a free-run case. The free-run is a pure LSM simulation without assimilating satellite data, but its model parameter values and forcing data are identical to the assimilation case. In principle, it is also necessary to compare the dual-pass assimilation case with a default-parameter-based assimilation case, but this was not conducted because of the difficulties involved in determining default parameters for the RTM.

4.1 Precipitation and soil water content

As near-surface soil moisture is strongly related to precipitation, errors in the input precipitation inevitably affect the accuracy of simulated soil moisture. Figure 3a shows numerous precipitation events in both the input GPCP data and observations at the BJ site

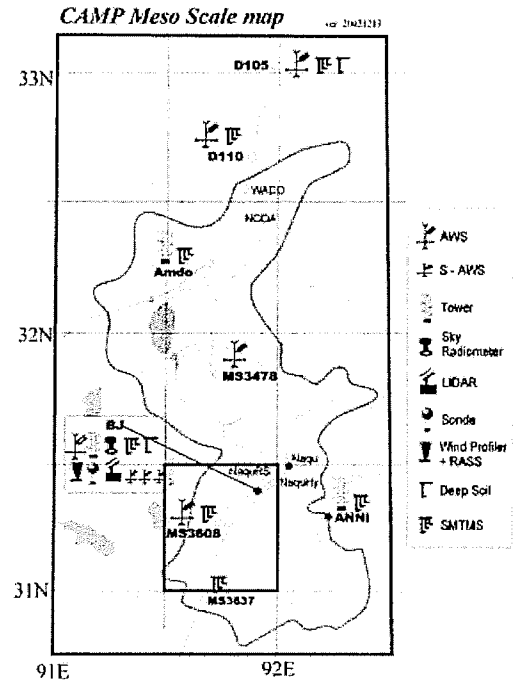

Fig. 2. Mesoscale map of the site of the CAMP/Tibet experiments. BJ is a CEOP reference site. The bold grid (hereafter termed the CEOP grid) is centered at (91.75°E, 31.25°N).

Table 1. Parameters measured at the CEOP East-Tibet reference site (BJ) in 2003. S-AWS1, S-AWS3, and SSMTMS are three stations located close to the BJ station.

Items	Station (depth)
Precipitation	BJ
Radiation	BJ
Surface temperature	BJ, MS3608 S-AWS1, S-AWS3
Near-surface soil moisture	BJ, MS3608 (4 cm) S-AWS1, S-AWS3 (0–5 cm) SSMTMS (0–3 cm)
Turbulent fluxes	BJ (3 m, 20 m)

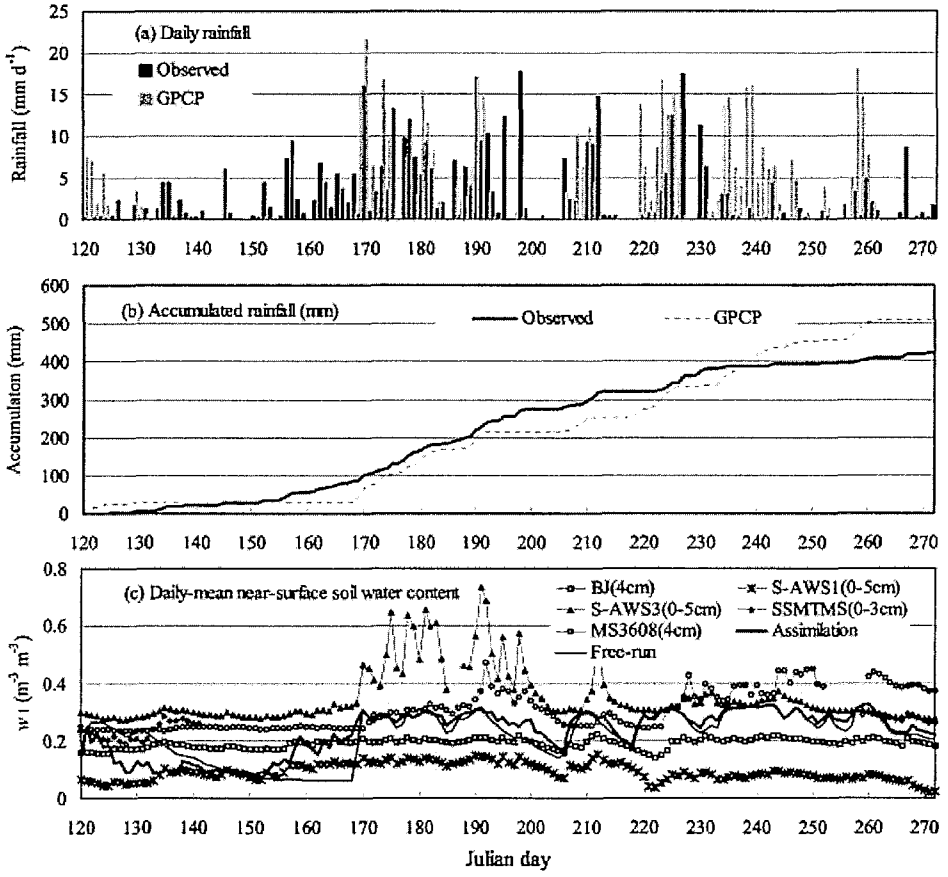

Fig. 3. (a) Daily mean precipitation in terms of both measurements and LDAS-UT input (GPCP); (b) Accumulated precipitation from Day 120; (c) Daily mean near-surface soil water content measured at five stations, LDAS-UT output, and free-run output for the CEOP grid from May to September 2003.

during Days 170–230; however, GPCP greatly underestimated the precipitation frequency and amount prior to Day 170 (June 19): the accumulated GPCP amount prior to Day 170 is 68 mm, whereas the measured amount is 104 mm (Fig. 3b). Figure 3c shows a comparison of the daily mean near-surface soil water content between the assimilation, the free-run, and observed measurements. Soil moisture was measured at five stations, which show significant variability in soil moisture within the CEOP grid. The values of soil moisture derived from the assimilation and the free-run show similar variations from Day 170 but differ for the period prior to Day 170. The free-run clearly shows a dry bias that lies outside the range of the variability during Days 150–170; this is the response of the LSM to the reduced precipitation input. In contrast, the soil moisture derived from the assimilation is situated within the observed range throughout the entire study period. In particular, LDAS-UT produced an increase in near-surface soil moisture during Days 150–170 in response to the measured precipitation, even though the measured precipitation was not included in the input data. In this way, the soil moisture derived from the assimilation system was corrected to some extent by assimilating microwave data. This makes the assimilation system less sensitive to the negative biases in input precipitation data than the free-run case.

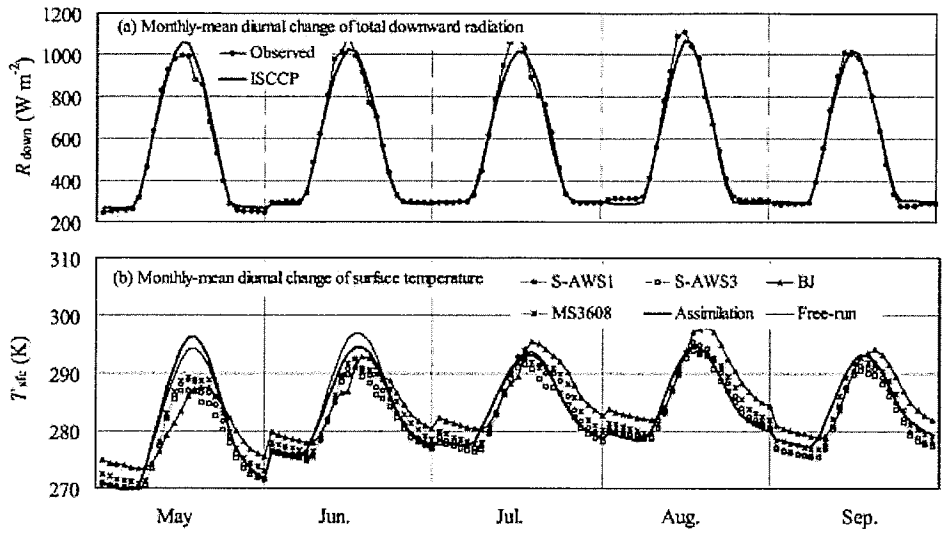

Fig. 4. (a) Comparison of monthly mean diurnal change in total downward radiation between values measured at the CEOP site and LDAS-UT input (ISCCP) for the CEOP grid; (b) Comparison of monthly mean diurnal change in surface temperature measured at four stations, LDAS-UT output, and free-run output for the CEOP grid from May to September 2003.

4.2 Downward radiation and surface temperature

Downward shortwave radiation and longwave radiation are important input parameters that affect the surface temperature (T_{sfc}) and surface energy partition. Figure 4a shows the monthly-mean diurnal variation in total (shortwave + longwave) downward radiation. The five-month mean value derived from ISCCP (528 W m^{-2}) is similar to measured values (531 W m^{-2}), but ISCCP yields a higher peak value in May and lower values in other months than observed data. Figure 4b shows the monthly mean diurnal variation in surface temperature. The diurnal change in T_{sfc} during May was overestimated by both the assimilation and the free-run. This overestimation resulted from a reduction in input precipitation, high input radiation, and the inability of the LSM to model freeze–thaw processes in soil. In June, the diurnal change in T_{sfc} continued to be overestimated because of the low amount of input precipitation, but LDAS-UT yielded much smaller errors than the free-run case. During July–September, both LDAS-UT and the free-run yielded surface temperatures that were similar to observed data.

4.3 Brightness temperature

Figures 5a,b shows the brightness temperature of 6.9 and 18.7 GHz vertical polarization, respectively. The root mean square error (*RMSE*) for the assimilation case and free case is also shown in the figure. The free-run yielded much stronger biases prior to Day 170, during which time precipitation data were missing in the input and the free-run produced a drier surface and higher brightness temperatures. In contrast, LDAS-UT yielded a wetter surface and more reasonable brightness temperature.

4.4 Surface energy budget

Sensible and latent heat fluxes at the study site were measured using the eddy-covariance method during an intensive observation period (Days 151–181) in 2003. Figures 6a–c show comparisons of net radiation, sensible heat, and latent heat, along with mean bias error (*MBE*) and root mean square error (*RMSE*).

The net radiation was basically reproduced in the assimilation and free-run cases, but peak values of net radiation were often underestimated; consequently, *RMSE* was as high as 89 W m^{-2} for both cases. This outcome is not unexpected, however, as the input ISCCP radi-

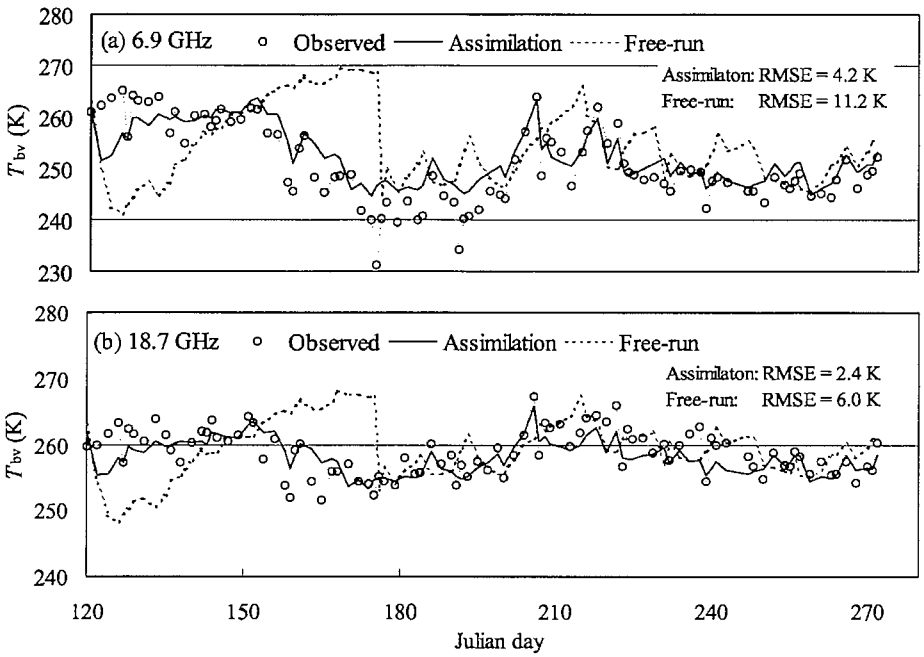

Fig. 5. Comparison of microwave brightness temperature derived from AMSR data, LDAS-UT output, and free-run output for the CEOP grid from May to September 2003. (a) 6.9 GHz vertical polarization; (b) 18.7 GHz vertical polarization. RMSE: root mean square error.

ation is a three-hourly mean in very large grids ($2.5° \times 2.5°$), meaning that the input radiation is effectively smoothed. The surface-emitted longwave radiation was better simulated in the assimilation case because of superior estimates of T_{sfc} (Fig. 4b). Accordingly, the net radiation was simulated more successfully in the assimilation than in the free-run.

In terms of the sensible and latent heat fluxes, the assimilation clearly produced better results than the free-run. In the assimilation case, the *RMSE* in hourly sensible heat fluxes (39 W m^{-2}) is much smaller than that for the free-run case (53 W m^{-2}), and the *RMSE* in latent heat fluxes (38 W m^{-2}) is also smaller than that for the free-run case (45 W m^{-2}). In addition, the monthly mean Bowen ratio (0.89) in the assimilation case is similar to the observed value (0.66), whereas that in the free-run case (1.22) is nearly double the observed value. In particular, when the observed precipitation was missing from the input data during Days 150–170, the free-run produced much higher sensible heat fluxes and much lower latent heat fluxes than observed values, while the assimilation produced much better surface energy partition. The relatively large errors in the free-run case result directly from the dry bias of soil moisture shown in Fig. 3(c). This result indicates that assimilating microwave data into a LSM can indirectly improve modeling of the surface energy budget by directly improving estimates of near-surface soil moisture.

5. Conclusions

The estimation of continuous regional soil moisture and the surface energy budget is crucial for studies of agricultural, hydrological, and atmospheric processes, as well as applied research. This study presented a land data assimilation system developed at The University of Tokyo that assimilates AMSR/AMSR-E low-frequency (6.9 and 18.7 GHz) brightness temperature into a LSM to improve the modeling of soil moisture and the surface energy budget. The data-assimilation system involves an embedded dual-pass technique. In Pass 1, key model parameters are automatically calibrated using satellite data and forcing data; Pass 2 produces the near-surface soil moisture and

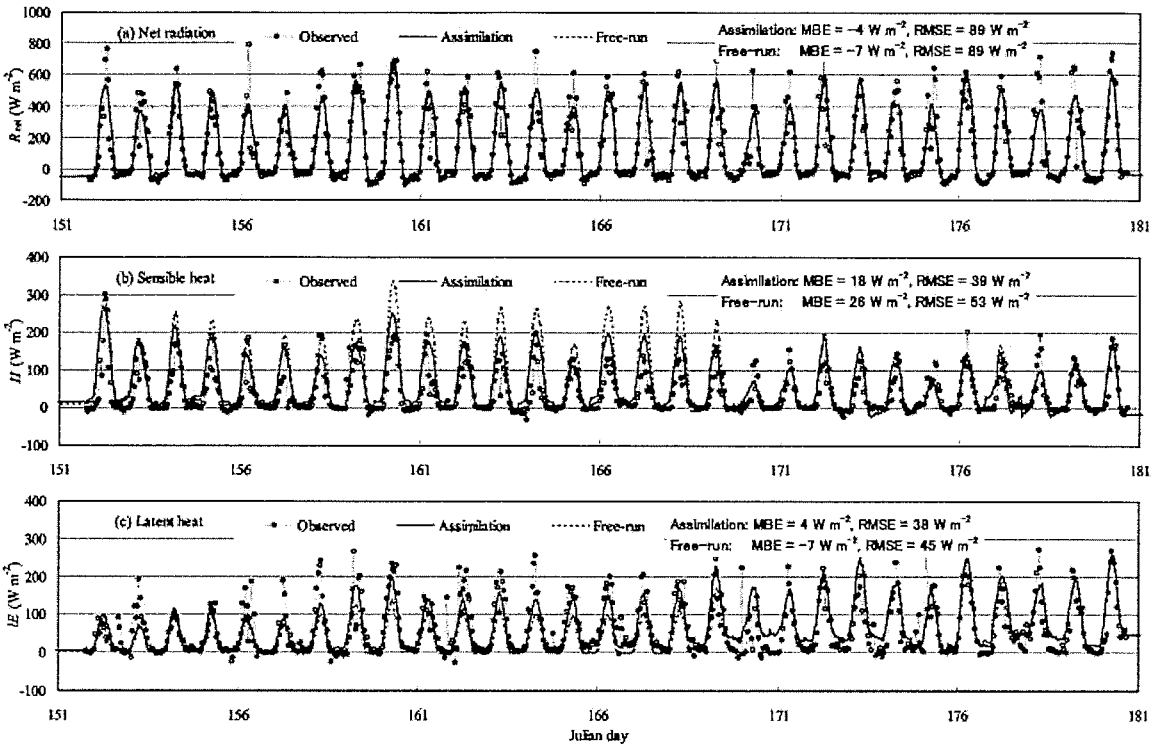

Fig. 6. Comparison of surface energy fluxes derived from measured values, LDAS-UT output, and free-run output for the CEOP grid in June 2003. (a) Net radiation; (b) Sensible heat flux; (c) Latent heat flux. *MBE*: mean bias error, *RMSE*: root mean square error.

surface energy budget by assimilating satellite data. As the system integrates well-established global products of soil, vegetation, precipitation, radiation, and other meteorological parameters, it is easily applied.

The system was evaluated using in situ data at a CEOP reference site. The results demonstrate that simulations of soil moisture and the surface energy budget were improved compared with the case with no assimilation. In particular, the soil moisture and energy partition simulated using the assimilation system is less contaminated by negative biases in input precipitation data than the case with no assimilation. This result is encouraging in terms of producing reliable surface-energy budgets in remote regions such as Tibet where precipitation-monitoring networks are sparse and input precipitation data are prone to large errors.

Although we presented clear evidence that the assimilation system is able to provide improved estimates of soil moisture and the surface energy budget, the system can be further improved in many respects. The following points are the major issues in terms of system performance. (1) The employed forcing data can be improved, as the system currently uses ISCCP coarse-resolution radiation data; these data can be replaced with radiation products with a higher spatial resolution once they are available and proven to be reliable. (2) The RTM only describes surface scattering, and it may fail for dry soil for which soil volumetric scattering makes a substantial contribution to the satellite-received radiance. This issue is currently under investigation; initial results can be found in Lu et al. (2006). (3) The LSM is unable to model soil freeze–thaw processes and should therefore be improved for applications in cold regions. (4) The future assimilation of remotely sensed surface temperature into the

system is likely to result in improved modeling of the surface energy budget. Efforts in these respects will contribute to improved system performance.

Acknowledgements

This study was funded by the Japan Science and Technology Agency and the Special Coordination Funds for Promoting Science and Technology. The in situ data used in this study were obtained from the CAMP/Tibet project. The authors would like to acknowledge Dr. Ken'ichi Ueno and other scientists involved in fieldwork. The GPCP precipitation data were provided by the NASA/Goddard Space Flight Center's Laboratory for Atmospheres, which develops and computes the data as a contribution to the GEWEX Global Precipitation Climatology Project. NCEP Reanalysis data were provided by the NOAA-CIRES ESRL/PSD Climate Diagnostics Branch, Boulder, Colorado, USA.

References

Berg, A.A., J.S. Famiglietti, J.P. Walker, and P.R. Houser, 2003: Impact of bias correction to reanalysis products on simulations of North American soil moisture and hydrological fluxes. *J. Geophys. Res.*, **108**(D16), 4490, doi:10.1029/2002JD003334.

Betts, A.K., 2004: Understanding hydrometeorology using global models. *Bull. Amer. Meteor. Soc.*, DOI:10.1175/BAMS-85-11-1673.

Betts, A.K., J.H. Ball, A.C.M. Beljaars, M.J. Miller, and P.A. Viterbo, 1996: The land surface-atmosphere interaction: A review based on observational and global modeling perspectives. *J. Geophys. Res.*, **101**(D3), 7209–7226.

Burke, E.J. and L.P. Simmonds, 2001: A simple parameterisation for retrieving soil moisture from passive microwave data. *Hydrol. Earth Syst. Sci.*, **5**, 39–48.

Clapp, R.B. and G.M. Hornberger, 1978: Empirical equations for some hydraulic properties. *Water Resour. Res.*, **14**, 601–604.

Cosby, B.J., G.M. Hornberger, R.B. Clapp, and T.R. Ginn, 1984: A statistical exploration of the relationships of soil moisture characteristics to the physical properties of soils. *Water Resour. Res.*, **20**, 682–690.

Crosson, W.L., C.A. Laymon, R. Inguva, and M.P. Schamschula, 2002: Assimilating remote sensing data in a surface flux-soil moisture model. *Hydrol. Process.*, **16**, 1645–1662.

Crow, W.T., R. Bindlish, and T.J. Jackson, 2005: The added value of spaceborne, passive microwave soil moisture retrievals for forecasting, rainfall-runoff partitioning. *Geophys. Res. Lett.*, **32**, L18401, doi:10.1029/2005GL023543.

Dirmeyer, P.A., A.J. Dolman, and N. Sato, 1999: The Pilot Phase of the Global Soil Wetness Project. *Bull. Amer. Meteor. Soc.*, **80**, 851–878.

Dobson, M.C., F.T. Ulaby, M.T. Hallikainen, and M.A. El-Rayes, 1985: Microwave dielectric behavior of wet soil—part II: dielectric mixing models. *IEEE Trans. Geosci. Remote Sens.*, **GE-23**, 35–46.

Duan, Q., V.K. Gupta, and S. Sorooshian, 1993: A shuffled complex evolution approach for effective and efficient global minimization. *J. Optimiz. Theory App.*, **76**, 501–521.

Dunne, S. and D. Entekhabi, 2005: An ensemble-based reanalysis approach to land data assimilation. *Water Resour. Res.*, **41**, W02013, doi:10.1029/2004WR003449.

Entekhabi, D., I. Rodriguez-Iturbe, and F. Castelli, 1996: Mutual interaction of soil moisture state and atmospheric processes. *J. of Hydro.*, **184**, 3–17.

Fujii, H., 2005: Development of a Microwave radiative transfer model for vegetated land surface based on comprehensive in-situ observations. PhD thesis, The University of Tokyo.

Gillies, R.R. and T.N. Carlson, 1995: Thermal remote sensing of surface soil water content with partial vegetation cover for incorporation into climate models. *J. Appl. Meteor.*, **34**, 745–756.

Global Soil Data Task, 2000: *Global Gridded Surfaces of Selected Soil Characteristics (IGBPDIS)*, International Geosphere-Biosphere Programme—Data and Information Services. Available online [http://www.daac.ornl.gov/] from the ORNL Distributed Active Archive Center, Oak Ridge National Laboratory, Oak Ridge, Tennessee, U.S.A.

Houser, P.R., W.J. Shuttleworth, J.S. Famiglietti, H.V. Gupta, K.H. Syed, and D.C. Goodrich, 1998: Integration of soil moisture remote sensing and hydrologic modeling using data assimilation. *Water Resour. Res.*, **34**, 3405–3420.

Huffman, G.J., R.F. Adler, M. Morrissey, D.T. Bolvin, S. Curtis, R. Joyce, B. McGavock, and J. Susskind, 2001: Global precipitation at one-degree daily resolution from multi-satellite observations. *J. Hydrometeor.*, **2**, 36–50.

Jackson, T.J., 1993: Measuring surface soil moisture using passive microwave remote sensing. *Hydro. Process.*, **7**, 139–152.

Jackson, T.J. and T.J. Schmugge, 1991: Vegetation effects on the microwave emission of soils. *Remote Sens. Environ.*, **36**, 203–212.

Johansen, O., 1975: *Thermal conductivity of soils.*

Ph.D. thesis, Trondheim, Norway (CRREL Draft translation 637, 1977).

Knyazikhin, Y., J. Glassy, J.L. Privette, Y. Tian, A. Lotsch, Y. Zhang, Y. Wang, J.T. Morisette, P. Votava, R.B. Myneni, R.R. Nemani, and S.W. Running, 1999: MODIS leaf area index (LAI) and fraction of photosynthetically active radiation absorbed by vegetation (FPAR) product (MOD15) algorithm theoretical basis document, pp. 126. Available online [http://eospso.gsfc.nasa.gov/atbd/modistables.html].

Koike, T., 2004: The Coordinated Enhanced Observing Period—an initial step for integrated global water cycle observation. *WMO Bulletin*, **53**(2), 1–8.

Koike, T., C. Shimo, T. Ohta, H. Fujii, and A. Shibata, 2000: Development and validation of a microwave radiometer algorithm for land surface hydrology. *Ann. J. Hydraulic Eng. JSCE*, **44**, 247–252.

Koster, R.D., P.A. Dirmeyer, Z. Guo, and the GLACE team co–authors, 2004: Regions of strong coupling between soil moisture and precipitation. *Science*, **305**, 1138–1140.

Loveland, T.R., B.C. Reed, J.F. Brown, D.O. Ohlen, J. Zhu, L. Yang, and J.W. Merchant, 2001: Development of a global land cover characteristics database and IGBP DISCover from 1-km AVHRR data. *Int. J. Remote Sensing*, **21**, 1303–1330.

Lu, H., T. Koike, N. Hirose, M. Morita, H. Fujii, D.N. Kuria, T. Graf, and H. Tsutsui, 2006: A basic study on soil moisture algorithm using ground based observations under dry condition. *Ann. J. Hydraul. Eng., JSCE*, **50**, 7–12.

Luo, L. and NLDAS team co–authors, 2003: Validation of the North American Land Data Assimilation System (NLDAS) retrospective forcing over the southern Great Plains. *J. Geophys. Res.*, **108**(D22), 8843, doi:10.1029/2002JD003246.

Ma, Y., H. Ishikawa, O. Tsukamoto, M. Menenti, Z. Su, T. Yao, T. Koike, and T. Yasunari, 2003: Regionalization of surface fluxes over heterogeneous landscape of the Tibetan Plateau by using satellite remote sensing data. *J. Meteor. Soc. Japan.*, **81**, 277–293.

Ma, Y., O. Tsukamoto, H. Ishikawa, Z. Su, M. Menenti, J. Wang, and J. Wen, 2002: Determination of regional land surface heat flux densities over heterogeneous landscape of HEIFE integrating satellite remote sensing with field observations. *J. Meteor. Soc. Japan*, **80**, 485–501.

Margulis, S.A., D. McLaughlin, D. Entekhabi, and S. Dunne, 2002: Land data assimilation and estimation of soil moisture using measurements from the Southern Great Plains 1997 Field Experiment. *Water Resour. Res.*, **38**, 1299, doi:10.1029/2001WR001114.

Meng, C.J., R.T. Pinker, J.D. Tarpley, and I. Laszlo, 2003: A satellite approach for estimating regional land surface energy budget for GCIP/GAPP. *J. Geophys. Res.*, **108**(D22), 8861, doi:10.1029/2002JD003088.

Mitchell, K.E. and NLDAS team co–authors, 2004: The multi-institution North American Land Data Assimilation System (NLDAS): Utilizing multiple GCIP products and partners in a continental distributed hydrological modeling system. *J. Geophys. Res.*, **109**, D07S90, doi:10.1029/2003JD003823.

Njoku, E.G. and D. Entekhabi, 1996: Passive microwave remote sensing of soil moisture. *J. Hydro.*, **184**, 101–129.

Paloscia, S., G. Macelloni, E. Santi, and T. Koike, 2001: A Multifrequency algorithm for the retrieval of soil moisture on a large scale using microwave data from SMMR and SSM/I satellites. *IEEE Trans. on Geosci. Remote Sensing*, **39**, 1655–1661.

Paloscia, S. and P. Pampaloni, 1988: Microwave polarization index for monitoring vegetation growth. *IEEE Trans. on Geosci. Remote Sensing*, **GE-26**, 617–621.

Parada, L.M. and X. Liang, 2004: Optimal multiscale Kalman filter for assimilation of near-surface soil moisture into land surface models. *J. Geophys. Res.*, **109**, D24109, doi:10.1029/2004JD004745.

Pathmathevan, M., T. Koike, and X. Li, 2003: A new satellite-based data assimilation algorithm to determine spatial and temporal variations of soil moisture and temperature profiles. *J. Meteor. Soc. Japan*, **81**, 1111–1135.

Pauwels, V.R.N., R. Hoeben, N.E.C. Verhoest, and F.P. De Troch, 2001: The importance of the spatial patterns of remotely sensed soil moisture in the improvement of discharge predictions for small-scale basins through data. *J. Hydro.*, **251**, 88–102.

Pitman, A.J. and PILPS team co–authors, 1999: Key Results and Implications from Phase 1(c) of the Project for Intercomparison of Land-surface Parameterization Schemes. *Clim. Dynamics*, **15**, 673–684.

Prigent, C., F. Aires, W.B. Rossow, and A. Robock, 2005: Sensitivity of satellite microwave and infrared observations to soil moisture at a global scale: Relationship of satellite observations to in situ soil moisture measurements. *J. Geophys Res.*, **110**, D07110, doi:10.1029/2004JD005087.

Owe, M., R. de Jeu, and J. Walker, 2001: A methodology for surface soil moisture and vegetation optical depth retrieval using the microwave

polarization difference Index. *IEEE Trans. on Geosci. Remote Sensing*, **39**, 1643–1654.

Reichle, R.H. and R.D. Koster, 2005: Global assimilation of satellite surface soil moisture retrievals into the NASA Catchment land surface model. *Geophys. Res. Lett.*, **32**, L02404, doi:10.1029/2004GL021700.

Reichle, R.H., D.B. McLaughlin, and D. Entekhabi, 2001: Variational data assimilation of microwave radiobrightness observations for land surface hydrology applications. *IEEE Trans. on Geosci. Remote Sensing*, **39**, 1708–1718.

Robock, A. and NLDAS team co–authors, 2003: Evaluation of the North American Land Data Assimilation System over the southern Great Plains during the warm season. *J. Geophys. Res.*, **108**(D22), 8846, doi:10.1029/2002JD003245.

Rodell, M, P.R. Houser, U. Jambor, J. Gottschalck, K. Mitchell, C.J. Meng, K. Arsenault, B. Cosgrove, J. Radakovich, M. Bosilovich, J.K. Entin, J.P. Walker, D. Lohmann, and D. Toll, 2004: The global land data assimilation system. *Bull. Amer. Meteor. Soc.*, **85**, 381–394.

Sellers, P.J., D.A. Randall, G.J. Collatz, J.A. Berry, C.B. Field, D.A. Dazlich, C. Zhang, G.D. Collelo, and L. Bounoua, 1996a: A revised land surface parameterization (SiB2) for atmospheric GCMs. Part I: Model formulation. *J. Climate*, **9**, 676–705.

Sellers, P.J., S.O. Los, C.J. Tucker, C.O. Justice, D.A. Dazlich, G.J. Collatz, and D.A. Randall, 1996b: A revised land surface parameterization (SiB2) for atmospheric GCMs. Part II: The generation of global fields of terrestrial biophysical parameters from satellite data. *J. Climate*, **9**, 706–737.

Shi, J.-C., L. Jiang, L. Zhang, K.-S. Chen, J.-P. Wigneron, and A. Chanzy, 2005: A parameterized multifrequency-polarization surface emission model. *IEEE Trans. on Geosci. Remote Sensing*, **43**, 2831–2841.

Ulaby, F.T., R.K. Moore, and A.K. Fung, 1986: Microwave Remote Sensing: Active and Passive. Volume III, from Theory to Applications, Artech House, Norwood, MA, pp 2162.

van den Hurk, B., 2001: Energy balance based surface flux estimation from satellite data, and its application for surface moisture assimilation. *Meteorol. Atmos. Phys.*, **76**, 43–52.

Vinnikov, K.Y., A. Robock, S.A. Qiu, J.K. Entin, M. Owe, B.J. Choudhury, S.E. Hollinger, and E.G. Njoku, 1999: Satellite remote sensing of soil moisture in Illinois, United States. *J. Geophys. Res.*, **104**(D4), 4145–4168.

Wang, J.R. and B.J. Choudhury, 1981: Remote sensing of soil moisture content over bare fields at 1.4 GHz frequency. *J. Geophys. Res.*, **86**, 5277–5282.

Watanabe, T. and J. Kondo, 1990: The influence of canopy structure and density upon the mixing length within and above vegetation. *J. Meteor. Soc. Japan.*, **68**, 227–235.

Wegmuller, U. and C. Matzler, 1999: Rough bare soil reflectivity model. *IEEE Trans. on Geosci. Remote Sensing*, **37**, 1391–1395.

Wetzel, P.J., D. Atlas, and R.H. Woodward, 1984: Determining soil moisture from geosynchronous satellite infrared data: a feasibility study. *J. Clim. Appl. Meteor.*, **23**, 375–391.

Wigneron, J.-P., A. Chanzy, J.-C. Calvet, and N. Bruguier, 1995: A simple algorithm to retrieve soil moisture and vegetation biomass using passive microwave measurements over crop fields. *Remote Sens. Environ.*, **51**, 331–341.

Yang, K., T. Koike, H. Fujii, K. Tamagawa, and N. Hirose, 2002: Improvement of surface flux with a turbulence-related length. *Q. J. R. Meteor. Soc.*, **128**, 2073–2087.

Yang, K., T. Koike, B. Ye, and L. Bastidas, 2005: Inverse analysis of the role of soil vertical heterogeneity in controlling surface soil state and energy partition. *J. Geophys. Res.*, **110**, D08101, doi:10.1029/2004JD005500.

Yang, K. and co–authors, 2007: Initial CEOP-based review of the prediction skill of operational general circulation models and land surface models. *J. Meteor. Soc. Japan*, this issue.

Zhang, S.-W., H.-R. Li, W.-D. Zhang, C.J. Qiu, and X. Li, 2006: Estimating the soil moisture profile by assimilating near-surface observations with the ensemble Kalman filter (EnKF). *Adv. Atmos. Sci.*, **22**, 936–945.

Zhang, Y., W.B. Rossow, A.A. Lacis, V. Oinas, and M.I. Mishchenko, 2004: Calculation of radiative fluxes from the surface to top of atmosphere based on ISCCP and other global data sets: Refinements of the radiative transfer model and the input data. *J. Geophys. Res.*, **109**, D19105, doi:10.1029/2003JD004457.